

RESEARCH

Open Access



# Depot-specific acetylation profiles of adipose tissues—therapeutic targets for metabolically unhealthy obesity

Haoyue Guo<sup>1†</sup>, Zhiyi Zhang<sup>2†</sup>, Juntao Yang<sup>2</sup>, Jiangfeng Liu<sup>2\*</sup>, Hongwei Lin<sup>3\*</sup> and Ningbei Yin<sup>1\*</sup>

## Abstract

**Background** Adipose tissue plays a critical role in the development of metabolically unhealthy obesity (MUO), with distinct adipose depots demonstrating functional differences. This study aimed to investigate the unique characteristics of subcutaneous (SA) and visceral adipose tissue (VA) in MUO.

**Methods** Paired omental VA and abdominal SA samples were obtained from four male patients with MUO and subjected to Four-Dimensional Data Independent Acquisition (4D-DIA) proteomic and lysine acetylation (Kac) analyses. Differentially expressed proteins and differentially modified Kac sites were identified, quantified, integrated, and subjected to functional analyses. Overlap analysis was performed between our datasets and previously published proteomic datasets in obesity populations. Additionally, differentially modified Kac sites on histones and their related enzymes were identified.

**Results** A total of 281 differentially expressed proteins and 147 differentially modified Kac sites were identified among 6,201 quantifiable proteins and 1,826 quantifiable Kac sites. Upregulated proteins and acetylated proteins in SA were predominantly enriched in extracellular matrix (ECM) remodeling pathways, while those in VA were enriched in energy metabolism and disease-related pathways. Differential ECM remodeling adaptability between SA and VA was primarily mediated by fibranexin and integrin, with COL6A1, COL6A3, and ITGA5 identified as differentially acetylated proteins overlapping between our dataset and previous studies. Potential unique proteins in MUO were enriched in inflammatory processes and closely associated with acetylated modifications. Specific differentially acetylated sites on histones, including H1.2K63, H1XK90, and H3.7K80, showed increased acetylation in VA, with N-deacetylase/N-sulfotransferase 1 (NDST1) identified as the associated enzyme.

**Conclusions** This study provided a comprehensive dataset on the proteomic and acetylomic profiles of SA and VA, laying a foundation for investigating the pathogenesis and potential therapeutic approaches for MUO. SA

<sup>†</sup>Haoyue Guo and Zhiyi Zhang are the co-first authors.

\*Correspondence:

Jiangfeng Liu

ljf@pumc.edu.cn

Hongwei Lin

linhw1973@126.com

Ningbei Yin

yinningbei@psh.pumc.edu.cn

Full list of author information is available at the end of the article



© The Author(s) 2025. **Open Access** This article is licensed under a Creative Commons Attribution-NonCommercial-NoDerivatives 4.0 International License, which permits any non-commercial use, sharing, distribution and reproduction in any medium or format, as long as you give appropriate credit to the original author(s) and the source, provide a link to the Creative Commons licence, and indicate if you modified the licensed material. You do not have permission under this licence to share adapted material derived from this article or parts of it. The images or other third party material in this article are included in the article's Creative Commons licence, unless indicated otherwise in a credit line to the material. If material is not included in the article's Creative Commons licence and your intended use is not permitted by statutory regulation or exceeds the permitted use, you will need to obtain permission directly from the copyright holder. To view a copy of this licence, visit <http://creativecommons.org/licenses/by-nc-nd/4.0/>.

was characterized by pronounced ECM remodeling regulation, while VA exhibited poorer adaptability and more prominent metabolic functional changes. These differential processes were influenced not only by protein expression levels but, more importantly, by acetylated modifications. The regulation of acetylated modifications in white adipose tissue (WAT), particularly for the differential Kac sites enriched in ECM remodeling and inflammation-related pathways, may serve as an effective intervention strategy for MUO, with NDST1 emerging as a promising therapeutic target.

**Trial registration** Not applicable since this study did not involve clinical intervention.

**Keywords** Proteome, Lysine acetylation, Metabolic syndrome, Metabolically unhealthy obesity, Adipose tissue

## Background

The World Obesity Federation published the latest World Obesity Atlas in 2024, entitled “Obesity and Its Resulting Diseases”, which emphasizes that obesity and related metabolic abnormalities are preventable [1]. Obesity is primarily characterized by an excessively high body mass index (BMI) and the over-accumulation of white adipose tissue (WAT). Metabolic syndrome (MetS) is defined by the clustering of key risk factors, including hypertension, insulin resistance, and dyslipidemia [2]. Individuals with obesity and MetS, collectively referred to as metabolically unhealthy obesity (MUO), are at a higher risk of all-cause mortality and exhibit a greater incidence of complications compared to individuals with non-obesity or metabolically healthy obesity (MHO) [1, 3]. Although individuals with MHO generally have a more favorable prognosis, approximately 50% progress to MUO over time [4]. Elucidating the pathological changes and molecular mechanisms in MUO is essential for preventing and managing related diseases.

Adipose tissue functions as a critical metabolic regulatory organ, playing a central role in maintaining systemic energy homeostasis. Alterations in WAT, particularly concerning proliferation, inflammation, metabolism, and endocrine regulation, are closely associated with obesity and related metabolic disorders [5]. WAT comprises visceral adipose tissue (VA) and subcutaneous adipose tissue (SA), which differ significantly in insulin sensitivity, lipid metabolism, and cytokine secretion [6]. While SA dysfunction and its associated ectopic lipid deposition are pivotal in the progression of metabolic disorders, VA is widely recognized as a potential predictor of MetS [7–9]. This study aimed to elucidate the distinct characteristics and regulatory mechanisms of SA and VA in obesity with MetS.

Advances in proteomic technologies have provided powerful tools to identify specific expression patterns across distinct adipose depots. Previous studies have investigated the differential expression between SA and VA in the context of obesity [10–18]. However, the specific molecular differences between SA and VA in obesity with MetS remain unclear. Moreover, prior studies were often constrained by the use of targeted methods for monitoring selected proteins or the limited sensitivity

of mass spectrometry [10]. Lysine acetylation (Kac), a prevalent post-translational modification, has extensive protein-level effects and plays a vital role in metabolic regulation [19]. Acetylation influences adipose tissue expansion, adipocyte differentiation, and adipokine secretion, making it a promising target for interventions aimed at obesity and related metabolic diseases [19–21]. This work integrated proteome and Kac analyses of VA and SA in individuals with MUO, providing a theoretical foundation for understanding pathological mechanisms and identifying potential interventions for MUO.

## Materials and methods

### Participants and sample collection

Paired omental VA and abdominal SA samples were collected from male patients with MUO undergoing laparoscopic sleeve gastrectomy at the Center for Obesity and Metabolic Disease, Plastic Surgery Hospital, Chinese Academy of Medical Sciences, and Peking Union Medical College. MUO was defined as obesity (BMI  $\geq 28$  kg/m<sup>2</sup>) accompanied by metabolic syndrome (MetS). MetS was diagnosed based on the modified NCEP ATP III criteria [22], requiring the presence of any three of the following five factors: abdominal obesity (waist circumference  $\geq 90$  cm for Asian men), hypertriglyceridemia (triglycerides  $\geq 1.7$  mmol/L), low HDL cholesterol (HDL cholesterol  $\leq 1.03$  mmol/L for men), elevated blood pressure (systolic blood pressure  $\geq 130$  mmHg and/or diastolic blood pressure  $\geq 85$  mmHg or current use of antihypertensive medication), and impaired fasting glucose (fasting plasma glucose  $\geq 5.6$  mmol/L). Exclusion criteria included: 1. History of non-primary bariatric surgery; 2. Presence of other diseases or a significant surgical history; 3. Regular use of medications. All participants provided written informed consent, and the study was approved by the hospital's Ethics Committee (2024 Registration No. (192)), in accordance with the Declaration of Helsinki.

### Samples processing

#### Protein extraction

Take an appropriate amount of samples, grind with liquid nitrogen, add an appropriate amount of SDS lysate (50mM Tris, 4%SDS), and swirl well. Centrifuge at 4°C,

14,000 g, 20 min, take supernatant. 10 $\mu$ L quantification, the rest frozen into  $-80^{\circ}\text{C}$ .

#### **Protein digestion and desalination**

Add the final concentration of 5mM DTT and incubate at  $37^{\circ}\text{C}$  for 30 min. The final concentration of 15mM IAA was added and the reaction was dark for 30 min. Add proper amount of cold methanol overnight. The next day, the supernatant was centrifuged at a high speed of 14,000 g at  $4^{\circ}\text{C}$ , the supernatant was discarded, 50mM ammonium bicarbonate was added into Trypsin (1:50), and the mixture was evenly mixed and incubated at  $37^{\circ}\text{C}$  overnight. The next day, after adding the final concentration of 1% FA, the supernatant was obtained by swirling for 5 min, centrifuging at  $4^{\circ}\text{C}$  at 16,000 g for 20 min.

The samples were desalted using a C18 column, 100% ACN activated the C18 column, 0.1% FA balanced the column, loading the sample onto the column, and then using 0.1% FA to wash the column to wash away impurities. Eluent was added to eluate the sample and freeze dried.

#### **Acetylated peptide enrichment**

Anti-acetyllsine antibody conjugated agarose beads (Micron Bio, #WM702) was used in the enrichment (without specified instructions to the compositions of buffer I-III). The peptide sample was added to the IP buffer to re-suspend the sample, and then centrifuged. Antibody beads were mixed well, washed with IP buffer, centrifuged at 2000 g for 1 min, and the supernatant was discarded. Add IP buffer, centrifuge 2000 g for 1 min, discard the supernatant, and clean for 3 times. The peptide solution was centrifuged at 14,000 g for 5 min, transferred to an EP tube containing Antibody beads, thoroughly mixed, and incubated at  $4^{\circ}\text{C}$  for 3 h. Centrifuge the beads 2000 g for 1 min to remove the supernatant. Add wash buffer I, mix thoroughly, centrifuge at 2000 g for 1 min, remove the supernatant, and repeat this step again. Add wash buffer II, mix thoroughly, centrifuge at 2000 g for 1 min, remove the supernatant; Add 500 $\mu$ L wash buffer III, mix thoroughly, centrifuge at 2000 g for 1 min, and remove the supernatant; 0.2% TFA was added into the EP tube, thoroughly mixed, incubated at room temperature for 10 min, and centrifuged at 2000 g for 1 min after incubation, the supernatant was transferred to the new EP tube for retention, and this step was repeated twice to combine the three supernatants. Centrifuge the combined supernatant of 10,000 g for 2 min and take the supernatant into a new EP tube for use. Finally, remove salt and freeze dried.

#### **LC-MS/MS analysis**

Prepare mobile phase A (100% water, 0.1% formic acid) and mobile phase B (80% acetonitrile, 0.1% formic acid).

Dissolve 10  $\mu$ L of mobile phase A in the lyophilized powder, and centrifuge at 14,000 g for 20 min at  $4^{\circ}\text{C}$ . Liquid Chromatograph Mass Spectrometer (LC-MS/MS) analysis of peptides was used on timsTOF-HT mass spectrometer (Bruker Corporation, Germany) coupled to UltiMate3000 high pressure system (Thermo Fisher Scientific). 400ng of peptides were loaded on a 15 cm column (100  $\mu$ m inner diameter, packed using ReproSil-Pur C18-AQ 1.5-  $\mu$ m silica beads; QL-HPLC-100\*15; Beijing Qinglian Biotech Co.,Ltd, Beijing, China). Peptides were separated using a gradient from 5 to 10% B in 4 min, then 10–24% B in 42 min, then 24–36% B in 7 min, 36–95% B in 1 min, holding it at 95% for 6 min. Use the timsTOF-HT mass spectromete with the Captive Spray ion source. Acquire mass spectra in Data-Independent Acquisition (DIA ) mode, with a mass scan range of m/z 300–1500. The resolution for the MS spectra was set to 60,000 (at m/z 1222). In the TIMS tunnel, set the accumulation time to 50 ms. The capillary voltage was set to 1.5 kV, with a mobility range of 0.7 to 1.3  $\text{cm}^2/(\text{V})$ . The total cycle time is 1.23 s.

#### **Data analysis**

##### ***The identification and quantitation of protein***

Mass spectrometry data were used the Spectronaut software. All searches were performed against the human UniProt reference proteome of canonical and isoform sequences with 20,434 entries downloaded in March 2024. Searches used carbamidomethylation as a fixed modification and acetylation of the protein N-terminus, oxidation of methionines and Acetyltion as variable modifications. Default settings were used for other parameters. In brief, a trypsin/P proteolytic cleavage rule was used, permitting a maximum of two miscleavages and a peptide length of 7–52 amino acids. Protein intensities were normalized using the “Local Normalization” algorithm in Spectronaut based on a local regression model. Spectral library generation stipulated a minimum of three fragments per peptide, and maximally, the six best fragments were included. A protein and precursor FDR of 1% were used and protein quantities were reported in samples only if the protein passed the filter. Multiple testing corrections were not applied due to the exploratory purpose of the study.

##### ***The functional analysis of protein and DEP***

Venn diagrams and chord plots were drawn using the Bioladder platform (<https://www.bioladder.cn/>), PCA analyses were performed using the R language FactoMineR package (version 2.11) and the factoextra package (version 1.0.7), and correlation analyses were performed using thepython package scipy (version 1.11.3),

The databases Kyoto Encyclopedia of Genes and Genomes (KEGG) and Reactome (<https://reactome.org>)

/) were used to analyze the protein family and pathway. Gene Ontology (GO) annotation of the proteome was derived from the GO database (<https://www.ebi.ac.uk/QuickGO/>). Proteins were classified by GO annotation based on three categories as follows: molecular function, biological process, and cellular component. PPI network analysis was performed using the string database (<https://cn.string-db.org/>), and the screening of acetylation-associated enzymes was performed with reference to the uniprot database (<https://www.uniprot.org/>).

The workflow was displayed in Fig. 1A.

## Results

### Participants and grouping

Paired VA and SA samples were collected from four male patients, with detailed demographic and clinical information provided in Table 1. The samples were subsequently subjected to proteomics and lysine acetylation analyses, with the grouping presented in Table 2.

### Identification of quantitative proteins and kac sites

A total of 6,201 proteins were identified, with 6,175 detected in VA and 6,158 in SA (Fig. 1B). Additionally, 1,810 Kac sites were observed on 864 acetylated proteins in SA, and 1,641 Kac sites on 813 acetylated proteins in VA (Fig. 1B). Furthermore, 26 proteins were exclusively expressed in SA and 43 in VA, while 185 specific Kac sites were detected in SA and 16 in VA (Fig. 1C). Pearson correlation analysis of the proteome and acetylome data revealed significant positive correlations both within and between groups, except for sample S1, which was identified as a potential outlier in the acetylation analysis (Fig. 1D). Hierarchical clustering and Principal Component Analysis (PCA) of the 6,132 proteins and 1,625 Kac sites detected in at least 50% of biological replicates demonstrated overall sample reproducibility. The proteomic data indicated partial separation between SA and VA samples, whereas the acetylomic data exhibited significant overlap between these groups, reflecting the complexity of their acetylation profiles (Fig. 1E).

### Proteome analysis

122 proteins were observed to be upregulated and 159 downregulated in VA compared to SA (Fig. 2A). The proteins with significant differential expression and their relative abundance levels were illustrated in Fig. 2B–C. The GO analyses showed that upregulated proteins in VA mainly involved in metabolic processes (including lipid metabolism, glucose metabolism, and cell respiration), with enrichment in mitochondria and lipid drop regions, and participated in kinds of oxidoreductase activities. Meanwhile, the upregulated proteins in SA mainly involved in biological processes related to ECM remodeling (including response to hypoxia, collagen catabolic

process, tissue remodeling, and extracellular matrix disassembly), with enrichment in ECM and cytoplasmic regions, and participated in signal recognition and transmission processes between cells, cells and extracellular matrix, and within the cellular matrix (Fig. 2D). The KEGG analyses revealed that the upregulated proteins in VA were mostly enriched in energy metabolism (Oxidative phosphorylation, and Thermogenesis) and disease pathways (various neurodegenerative diseases, nonalcoholic fatty liver disease) (Fig. 2E), while the upregulated proteins in SA were mostly enriched in pathways related to extracellular matrix remodeling (ECM-receptor interaction, PI3K-Akt signaling pathway, Focal adhesion, and TGF-beta signaling pathway), with a chord plot displaying the proteins involved in the corresponding pathways (Fig. 2F).

### Acetylome analysis

A total of 86 downregulated and 61 upregulated Kac sites were identified in VA compared to SA (Fig. 3A). The Kac sites with significant differences and their relative levels are illustrated in Fig. 3B and C. GO analysis revealed that the upregulated Kac sites in VA were primarily involved in the translation and expression of genetic information, enriched in cytosolic and ribosomal regions, and predominantly participated in information processing. In contrast, the upregulated Kac sites in SA were associated with biological processes, cellular regions, and molecular functions related to ECM remodeling (Fig. 3D). KEGG pathway analysis further demonstrated that the upregulated Kac sites in VA were mainly enriched in pathways related to the ribosome, COVID-19, and metabolism, particularly glucose and amino acid metabolism (Fig. 3E). Meanwhile, the upregulated Kac sites in SA were predominantly associated with pathways involved in ECM remodeling and lipid metabolism (Fig. 3F).

### Integrative proteome and acetylome analysis

To further investigate the molecular regulation in MUO, an integrative global analysis combining proteome and acetylome datasets was conducted. A total of 781 overlapping acetylated proteins were identified, accounting for 12.66% of the quantifiable proteins and 91.35% of the quantifiable acetylated proteins (Fig. 4A). Pearson correlation analysis demonstrated positive correlations across all samples, both within and between the two groups (Fig. 4B). A nine-quadrant integrative diagram was constructed to compare differences in protein expression and Kac modification levels between VA and SA (Fig. 4C). The analysis focused on acetylated proteins with differential Kac modification levels between SA and VA, as well as their enriched pathways identified through KEGG analysis. Notably, acetylated proteins with downregulated Kac modification levels and either downregulated

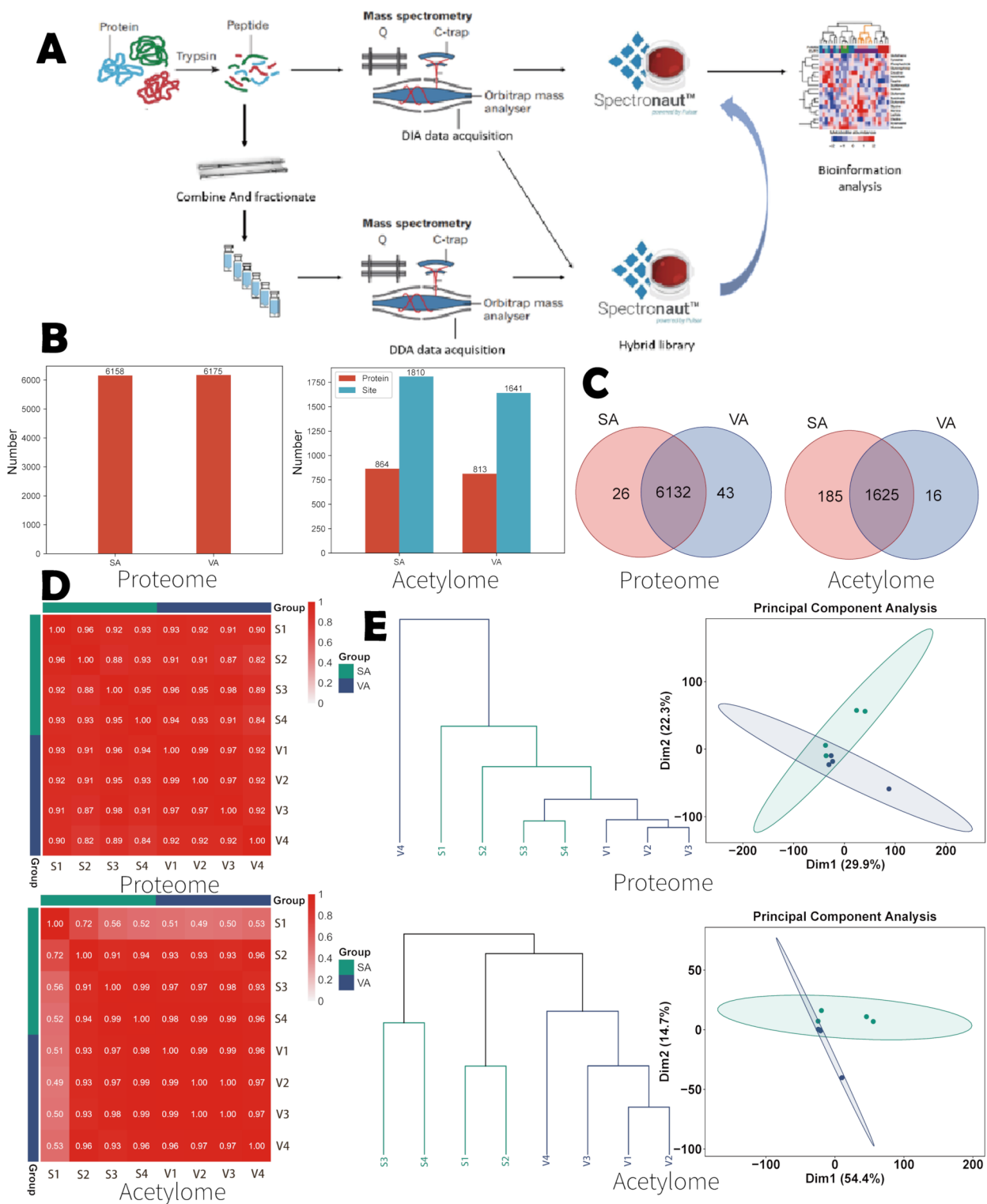


**Fig. 1** Overview of proteome and acetylome analysis. (1 **A\***) The workflow. (1 **B\***) Identified proteins/ Kac sites. (1 **C\***) Venn diagram of the overlaps across groups. (1 **D\***) Pearson correlation analysis of identified proteins/ Kac sites between samples across groups. (1 **E\*\***) Hierarchical clustering and Principal Components Analysis. \*Proteins/sites with intensity in at least one sample. \*\*Proteins/sites with intensity in at least 50% samples, with missing values filled using minimum value after median normalization across columns

**Table 1** Demographics and clinical information of participants

No	1	2	3	4
age (y)	33	46	31	30
BMI(kg/m <sup>2</sup> )	39.20	35.02	40.00	36.80
Waist(cm)	129	122	116	121
History of high blood pressure*	1	1	1	1
Systolic blood pressure (mmHg)	143	131	122	138
Diastolic blood pressure (mmHg)	87	84	82	96
History of diabetes*	0	1	1	0
Fasting plasma glucose (mmol/L)	6	9.1	6.2	5.1
Serum insulin (mU/L)	19.9	14.2	32.6	17
OGTT (Oral Glucose Tolerance Test)				
0 h glucose (mmol/L)	6.7	9.3	7.3	5.3
2 h glucose (mmol/L)	10.4	11.2	12.5	9.1
HbA1c (%)	4.75	7.9	6.3	4.63
HOMA-IR	5.31	5.74	8.98	3.85
Plasma HDL cholesterol (mmol/L)	1.06	1.05	1	0.71
Plasma LDL cholesterol (mmol/L)	3.21	3.59	2.87	4.83
Plasma total cholesterol (mmol/L)	4.80	4.68	5.97	6.64
Plasma triglycerides (mmol/L)	2.09	1.51	2.74	4.08

\* "1" indicated "with history of high blood pressure/ diabetes", "0" indicated "without history of high blood pressure/ diabetes"

**Table 2** Overview of samples Grouping and Biological replicates

Types of Omics	VA	SA
Proteome	4	4
Lysine Acetylation	4	4

or unchanged expression levels in VA (quadrants 7 and 8), including COL6A1, COL6A2, COL6A3, COL12A1, COL14A1, TNXB, FBN1, DCN, ALDOC, PFKF, and ITGA5, were predominantly enriched in pathways related to ECM remodeling (Fig. 4D).

### Overlap analysis with previous study

The referenced study [23] conducted a comprehensive untargeted proteomics analysis on paired SAT and VAT biopsies from 16 male and 16 female patients with severe obesity. Quantification retained proteins identified in at least eight samples from each of the four experimental groups (SAT-female, SAT-male, VAT-female, VAT-male), resulting in a final dataset of 4,506 proteins for downstream analysis. In contrast, our study quantified 6,201 proteins and 1,826 acetylated proteins. An overlap comparison revealed that 4,010 proteins were commonly identified between the two studies, as shown in a Venn diagram. Considering the critical role of acetylation in adipose tissue metabolism, we focused specifically on acetylated proteins shared between the two datasets, identifying 1,227 overlapping acetylated proteins (Fig. 5A). Among MUO patients in our study, 31 acetylated proteins were upregulated, and 38 were downregulated in VA. Notably, COL6A1, COL6A3, and ITGA5 were overlapping acetylated proteins that were not only differentially acetylated between VA and SA in MUO but

also identified in individuals with obesity (Fig. 5A). This finding further confirmed that these differentially acetylated proteins, enriched in ECM remodeling pathways, contributed to the differences between the two adipose depots.

Additionally, our study identified 1,592 non-acetylated proteins and 599 acetylated proteins unique to MUO patients compared to the proteome dataset of VA and SA in individuals with obesity. GO and Reactome analyses of these newly identified proteins revealed distinct functional roles. The 1,592 newly identified non-acetylated proteins were primarily involved in processes related to mitochondrial ribosomal genetic information transmission (Fig. 5B), whereas the 599 newly identified acetylated proteins were predominantly associated with inflammatory and immune-related processes (Fig. 5C).

### Histone acetylated modification

The quantities of Kac modifications on linker histone H1 and core histones H2A, H2B, H3, and H4 were 6, 10, 9, 18, and 16, respectively (Fig. 6A). A significant difference in the acetylation levels of histone H2A was observed between SA and VA ( $p < 0.05$ ; Fig. 6B). Specific differentially acetylated sites, including H1.2K63, H1XK90, and H3.7K80, predominantly exhibited upregulated acetylation in VA (Fig. 6C). N-deacetylase/N-sulfotransferase 1 (NDST1) was identified as the enzyme responsible for these differentially acetylated Kac sites on histones. This identification was based on differential expression data, the UniProt database, and prior studies (Fig. 6D). Pearson correlation analysis revealed positive correlations between NDST1 and the differentially acetylated Kac sites, with a particularly strong correlation observed with H1XK90 (Fig. 6E).

### Discussion

This study significantly expanded the proteomic and acetylomic datasets of human adipose tissue compared to previous studies [10–21]. Functional alterations in WAT were closely associated with the progression of obesity and metabolic disorders. A positive energy balance leads to lipid accumulation in WAT, and excessive expansion is accompanied by structural remodeling and functional changes, including angiogenesis disorders, adipocyte hypoxia and necrosis, macrophage infiltration, inflammation, and fibrosis. Concurrently, excess lipids may accumulate ectopically in VA, the liver, and other organs [24, 25]. Previous studies have identified structural, functional, and metabolic regulatory differences between SA and VA [6, 26]. This study aimed to elucidate the distinct characteristics of SA and VA in MUO, explore underlying mechanisms, and identify potential intervention targets associated with the differential regulation between SA and VA through integrative proteomic and acetylomic

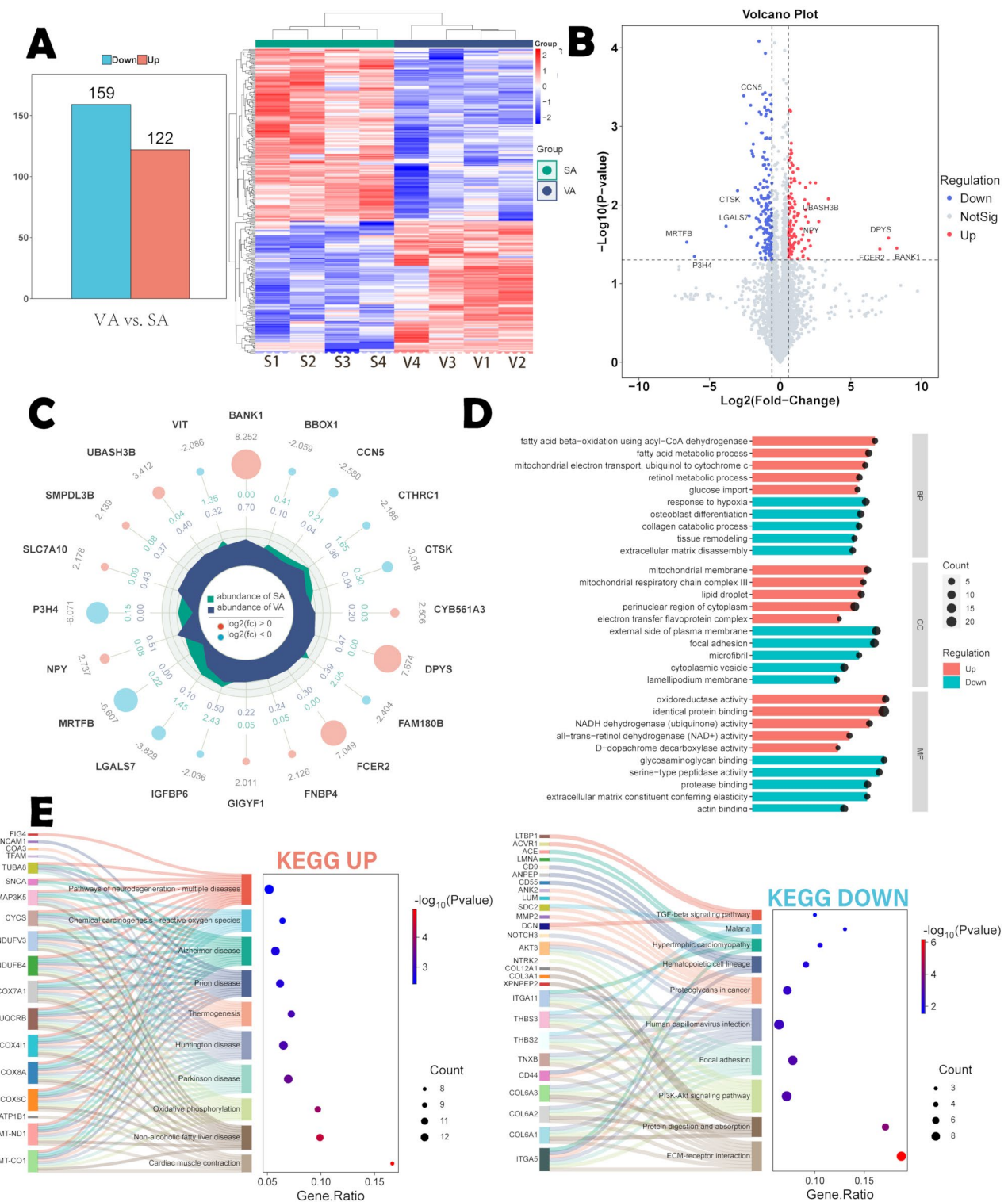


**Fig. 2** Proteome analysis. (2 **A**) 159 downregulated and 122 upregulated proteins in VA compared to SA. Correlation analysis was shown in the heatmap dia gram. (2 **B**) The top 5 upregulated (red) and downregulated (blue) proteins in VA compared to SA were shown in the volcano plot. (2 **C**) The top 10 upregulated (red) and downregulated (blue) proteins were shown in the radar plot, with the second ring showed the log2-transformed FC values, and the third ring represented the average quantification levels. (2 **D**) GO enrichment for BP, CC, and MF categories, selecting the top 5 upregulated (red) and downregulated (blue) pathways in VA compared to SA for each category, longer bars indicated smaller p-values while larger points represented more genes. (2 **E**) KEGG enrichment bubble chart (right) combined with a Sankey-bubble plot (left). The Sankey plot represented proteins included in each pathway, while the bubble plot displayed bubble size as the number of proteins in the pathways and bubble color as the p-value. The top 10 upregulated and downregulated pathways were selected for visualization

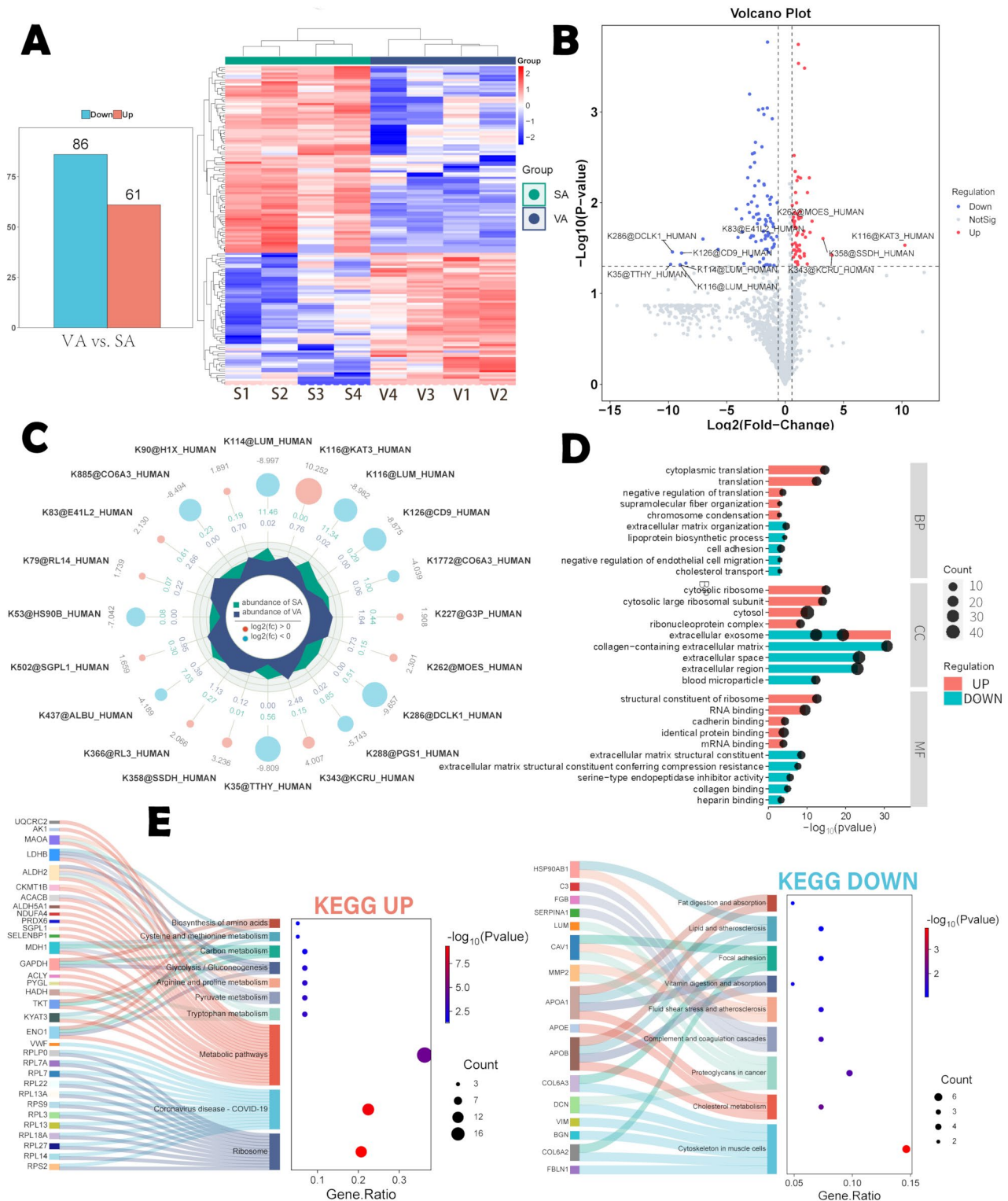


**Fig. 3** Acetyome analysis. (3A) 86 downregulated and 61 upregulated Kac sites in VA compared to SA. Correlation analysis was shown in the heatmap dia gram. (3B) The top 5 upregulated (red) and downregulated (blue) Kac sites in VA compared to SA were shown in the volcano plot. (3C) The top 10 upregulated (red) and downregulated (blue) Kac sites were shown in the radar plot, with the second ring showed the  $\log_2$ -transformed FC values, and the third ring represented the average quantification levels. (3D) GO enrichment for BP, CC, and MF categories, selecting the top 5 upregulated (red) and downregulated (blue) Kac sites in VA compared to SA for each category, longer bars indicated smaller p-values while larger points represented more genes. (3E) KEGG enrichment bubble chart (right) combined with a Sankey-bubble plot (left). The Sankey plot represented acetylated proteins included in each pathway, while the bubble plot displayed bubble size as the number of acetylated proteins in the pathways and bubble color as the p-value. The top 10 upregulated and downregulated pathways were selected for visualization

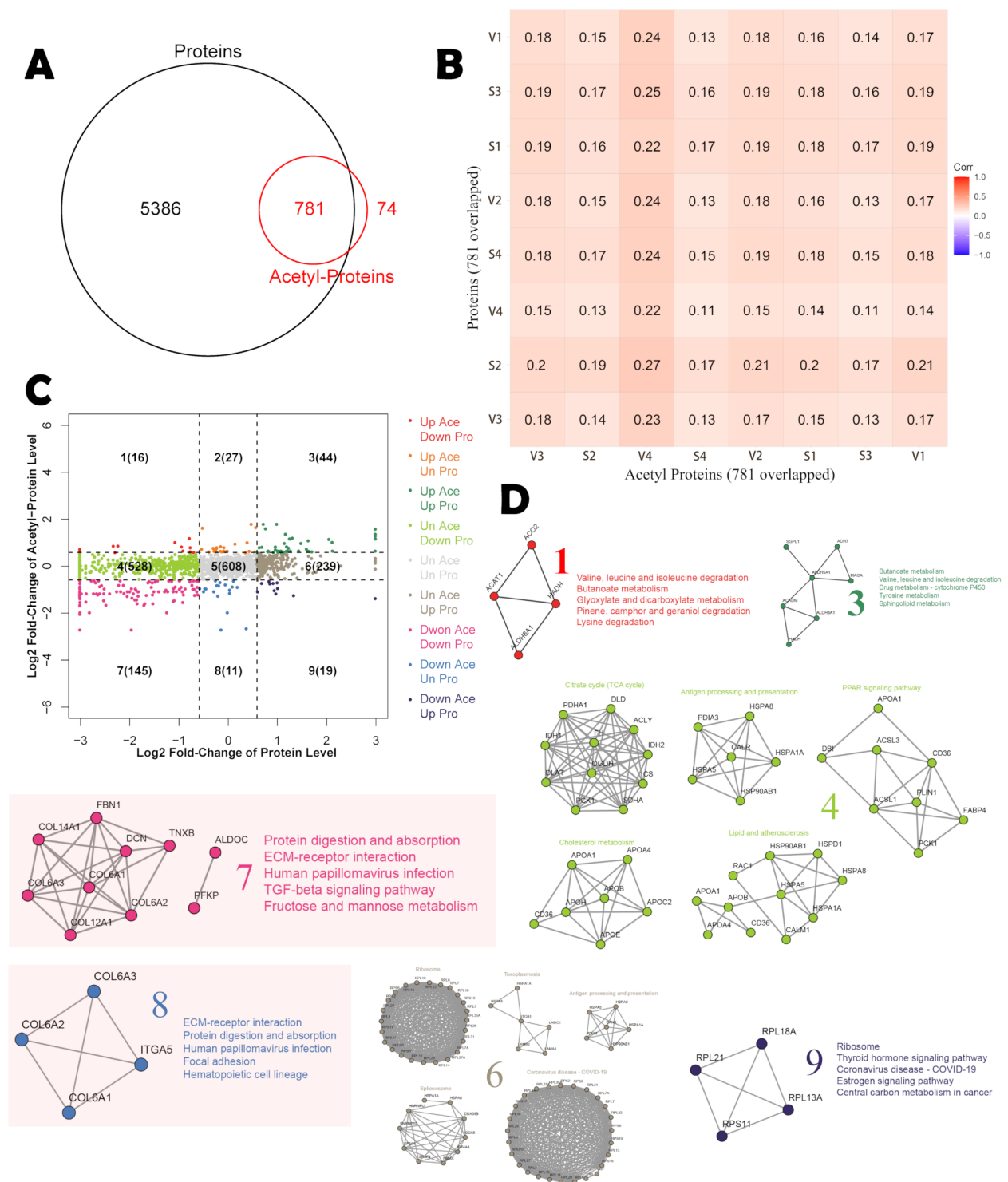


**Fig. 4** Integrative proteome and acetylome analyses. (4 **A**) 6167 proteins and 855 acetylated proteins with intensity in more than 50% of the replicates were identified, with 781 proteins duplicated and shown in Venn Diagram. (4 **B**) Correlation analysis of between quantifiable proteins/ acetylated proteins and the 781 overlapped acetylated proteins were shown in the heatmap diagram. (4 **C**) Nine-quadrant plots diagram for integrative analyses of proteome and acetylome. (4 **D**) Proteins from the KEGG significantly enriched top 5 pathways were extracted in the eight regions outside the central area of Fig. 4C. PPI networks for the selected proteins were constructed and visualized in each region, with part 2 did not generate a PPI network. The selected proteins of part 7 and 8 were mainly enriched in pathways related to ECM remodeling

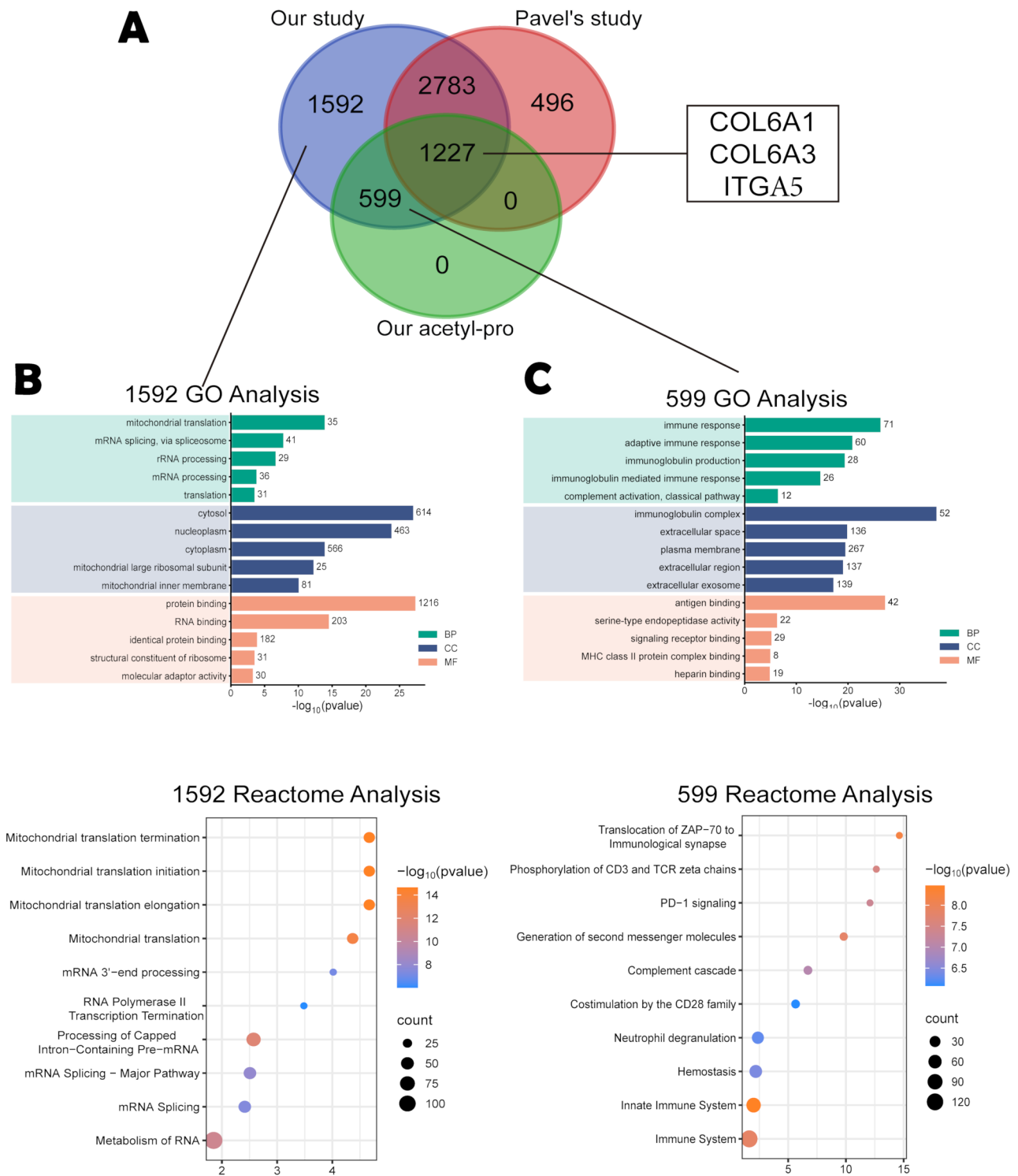


**Fig. 5** Overlap analysis with previous study. (5 **A**) The Venn diagram illustrated the overlap between the datasets of the two studies. COL6A1, COL6A3, and ITGA5 were discovered as the overlapping acetylated proteins. (5**B**) GO and REACTOME pathway enrichments of the 1592 newly identified non-acetylated proteins in MUO. (5 **C**) GO and REACTOME pathway enrichments of the 599 newly identified acetylated proteins in MUO

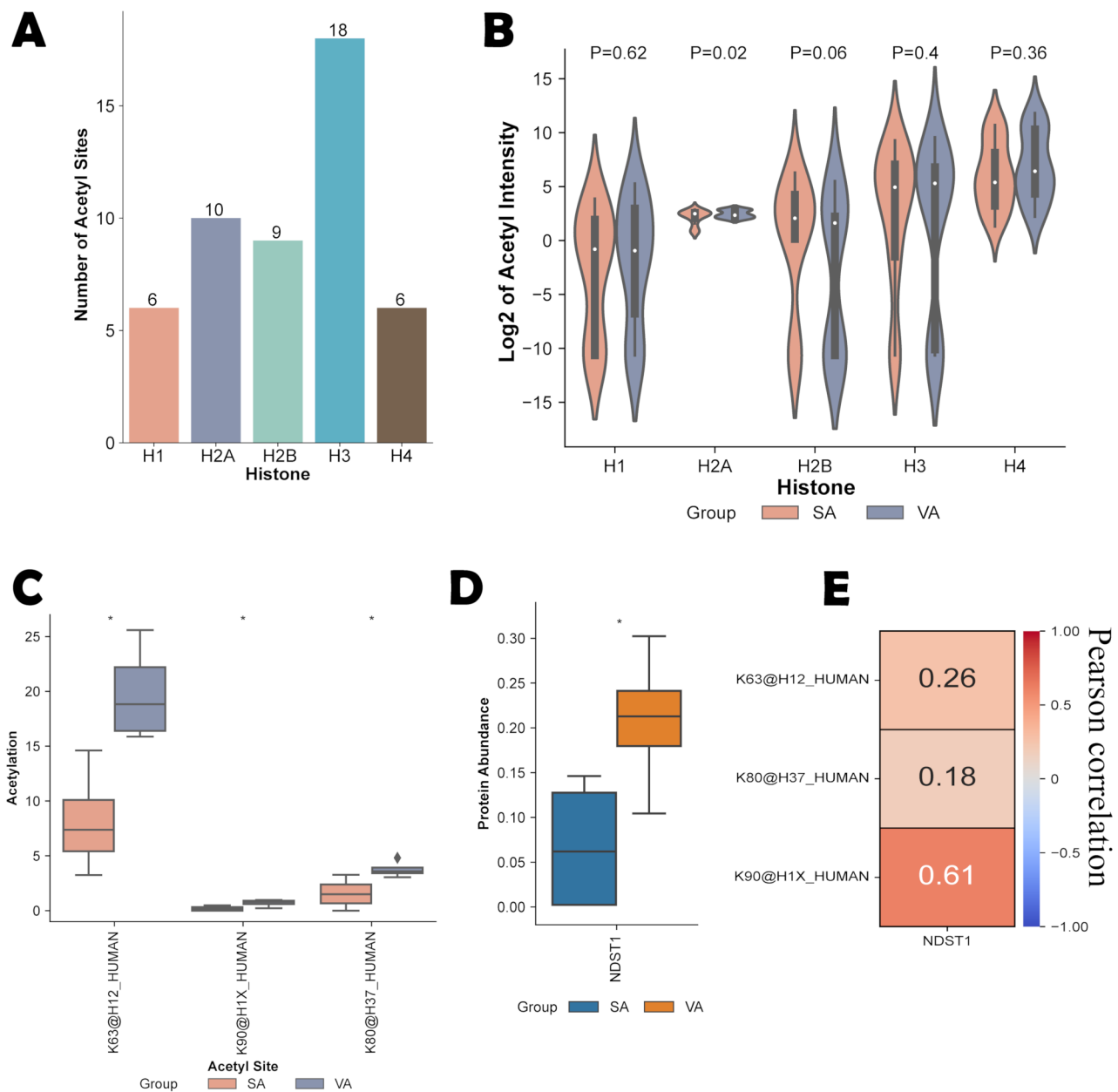


**Fig. 6** Histone acetylated modification. (6A) Number of Kac modifications on histones. (6B) Differences on acetylation levels of histones between VA and SA. (6C) Kac sites on histones with significant differences in acetylation levels. \* denoted  $p$ -value < 0.05. (6D) NDST1 was selected as the target enzyme with the abundant differences in the box plot. (6E) Pearson correlation analysis demonstrated positive correlations between NDST1 and the differentially acetylated Kac sites, particularly with H1XK90

analyses. While proteomic data suggested some degree of separation, the acetylomic results underscored nuanced differences between SA and VA. This highlighted the diversity and complexity of acetylation modifications, as well as the shared acetylated features across different samples. Subsequent functional enrichment analyses were conducted to explore the regulatory mechanisms of acetylation modifications in greater depth, aiming to better understand their roles in biological processes.

The ECM, a dynamic structure composed of macromolecules secreted by cells into the extracellular interstitium, remodels to accommodate lipid droplet growth during adipose tissue expansion [27, 28]. ECM remodeling is tightly regulated by focal adhesion, which mediates bidirectional physical communication between cells and the ECM [29]. During obesity, the overgrowth and altered secretion profile of adipocytes lead to and are influenced by ECM remodeling through: (1) adipose tissue fibrosis

caused by excessive ECM synthesis and cross-linking, in which the TGF- $\beta$  signaling pathway plays a key role [30], and (2) inflammation in adipose tissue, induced and exacerbated by ECM remodeling, resulting from local hypoxia and mechanical stress [27]. ECM remodeling is also intricately regulated by insulin and metabolism, with the PI3K signaling pathway playing a central role. Insulin binding to adipocyte receptors stimulates glucose uptake and glycolysis via the PI3K-Akt-mTORC1/GSK3 pathways and promotes lipid synthesis while inhibiting lipolysis via the PI3K-AKT-SREBP-1c/FOXO1 pathways. Dysfunctional adipocytes result in insulin resistance and metabolic disorders [31–33].

The upregulated differential proteins and acetylated proteins in SA were predominantly enriched in ECM remodeling-related pathways, while those in VA were enriched mainly in metabolic pathways. These findings confirmed the existence of differential expression and acetylation regulation patterns between SA and VA in MUO, highlighting the superior expansion and remodeling ability of SA and the poor adaptability of VA, which leads to rapid functional deterioration. Enhancing the ECM microenvironment in SA to sustain its energy storage capacity and compensatory role in obesity, while mitigating lipid toxicity by promoting remodeling regulation in VA, may represent potential intervention strategies for MUO. Notably, upregulated Kac sites in VA were significantly enriched in the COVID-19 pathway. Previous transcriptomic studies have shown that a history of COVID-19 can affect the transcriptome of WAT with depot-specific differences [34]. Our study provided protein-level evidence for the differential effects of COVID-19 on distinct WAT depots and underscored the critical role of acetylation modifications.

COL6A1, COL6A3, and ITGA5 were validated as potential targets for regulating the ECM remodeling process, as they were upregulated in SA compared to VA and overlapped with both our dataset and previous proteomic studies [23]. COL6A1 and COL6A3 are predominant ECM constituents, playing critical roles in regulating fibrotic changes, tissue rigidity, inflammatory responses, adipocyte expandability, and insulin sensitivity in WAT [28, 30, 35]. ITGA5, a member of the integrin family, acts as a fibronectin receptor in the ECM and is involved in adipocyte differentiation, ECM remodeling, inflammatory microenvironment modulation, and metabolic regulation in WAT [36, 37]. Elevated COL6 expression in SA has been reported in patients with type 2 diabetes (T2D) [23], while increased ITGA5 expression in SA has been observed in obese individuals [38]. Overlapping analyses reinforced the existence of differential regulation in ECM remodeling processes, primarily mediated by fibronectin and integrin, between SA and VA in obese individuals. Our findings further confirmed that

these differential regulations were influenced not only by protein expression levels but also by acetylation modifications, emphasizing the critical role of post-translational Kac modifications in obesity and metabolic disorders.

Notably, this study identified 599 acetylated proteins in adipose tissue that were not present in a previous dataset from obese patients [23]. These acetylated proteins were enriched in inflammation- and immune-related pathways, further highlighting the critical role of inflammation in adipose tissue in the development of obesity-associated metabolic disorders, consistent with prior studies [5, 27]. Our study confirmed that inflammation in WAT is closely correlated with acetylation modifications and provided potential acetylation modification targets. Future studies could explore effective interventions for MetS in obese populations by focusing on Kac sites enriched in ECM remodeling and inflammation-inducing pathways in WAT.

Histone acetylation is critical for adipose tissue expansion, lipid metabolism, and insulin resistance, making it a potential target for preventing obesity and related metabolic abnormalities [21, 39, 40]. Our analysis revealed that differentially modified Kac sites on histones, including H1.2K63, H1XK90, and H3.7K80, were significantly upregulated in VA. H1.2K63 has been identified as a non-proteolytic ubiquitylation target triggered by DNA double-strand breaks, facilitating the recruitment of DNA repair factors [41]. In contrast, the Kac modification of H1X and H3.7 has not been comprehensively investigated. Glucosamine NDST1 was identified as a key enzyme associated with these differentially acetylated histone Kac sites. NDST1 may regulate intracellular lipid metabolism and autophagy by controlling heparan sulfate chain modifications [42], and reduce fibrosis in adipose-derived stem cells when overexpressed [43]. While NDST1 represents a potential intervention target for MUO, the role of NDST1-associated histone Kac sites, such as H1XK90, in chromatin remodeling and metabolic regulation requires further investigation.

Metabolic syndrome represents a cluster of interconnected metabolic risk factors, often varying significantly among individuals. Our findings suggested that adipose tissue-specific pathways were relatively robust and function independently of systemic metabolic variability, as evidenced by the high intercorrelation of protein abundance and acetylation profiles among subjects with distinct metabolic characteristics. Consistent with recent transcriptomic datasets of adipose tissue in MHO and MUO populations [44], our findings highlighted shared regulatory mechanisms within adipose tissue and emphasized the necessity for further analyses at the single-cell level. Integrating our findings with prior proteomic datasets [23, 45], we proposed that mitochondrial dysfunction related to non-acetylated proteins and

inflammation dysregulation related to acetylated proteins were key molecular characteristics of MUO adipose tissue. These processes collectively contributed to metabolic dysregulation through impaired energy metabolism, oxidative stress, and chronic low-grade inflammation. Targeting these pathways, especially depot-specific acetylation modifications in adipose tissue, may represent a promising therapeutic approach for managing metabolic disorders in MUO patients.

This study has several limitations. A limited sample size of male patients was analyzed, avoiding the effects of gender but reducing the generalizability of our findings. Additionally, the lack of multiple testing corrections increased the risk of false positives but ensured that potential targets were not prematurely excluded. This study served as an initial exploration to identify potential targets and generate hypotheses for future research. Validation and mechanistic studies, though important, were not included. Future studies with larger, more diverse cohorts, including female participants, are needed to validate these findings and enhance their generalizability.

## Conclusions

This study provided comprehensive proteomic and lysine acetylation data for SA and VA, establishing a robust foundation for understanding the pathogenesis and potential treatment strategies for MUO. SA was characterized by stronger regulation of ECM remodeling, whereas VA exhibited poorer adaptability and more pronounced metabolic functional changes. The differential ECM remodeling processes in SA and VA were primarily mediated by fibranexin and integrin, with COL6A1, COL6A3, and ITGA5 identified as potential targets. These targets were influenced not only by protein expression levels but, more critically, by acetylation modifications. The regulation of acetylation modifications in WAT, particularly at differential Kac sites enriched in ECM remodeling and inflammation-inducing pathways, represents a promising intervention strategy for MUO, with NDST1 identified as a potential target.

## Abbreviations

BMI	Body mass index
4D-DIA	Four-Dimensional Data Independent Acquisition
DIA	Data Independent Acquisition
Kac	lysine acetylation
KEGG	Kyoto encyclopedia of genes and genomes
GO	Gene Ontology
MetS	Metabolic syndrome
MHO	Metabolically healthy obesity
MUO	Metabolically unhealthy obesity
SA	Subcutaneous adipose tissue
VA	Visceral adipose tissue
WAT	White adipose tissue
COL6A1/A2/A3	Collagen 6 A1/2/3
ITGA5	Integrin Subunit Alpha 5
COL12A1	Collagen 12 A1
COL14A1	Collagen 14 A1

TNXB	Tenascin XB
FBN1	Fibrillin 1
DCN	Decorin
ALDOC	Aldolase, Fructose-Bisphosphate C
PFKP	Phosphofructokinase, Platelet

## Acknowledgements

Not applicable.

## Author contributions

Ningbei Yin, Hongwei Lin and Jiangfeng Liu designed the study, directed the research and contributed to the critical revision of the article. Haoyue Guo and Zhiyi Zhang conducted the experiments, analyzed the data, and wrote the manuscript. Juntao Yang supervised the research, performed data management and assisted with the completion of the manuscript.

## Funding

This work was supported by Chinese Academy of Medical Sciences Initiative for Innovative Medicine (2021-I2M-1-052).

## Data availability

The mass spectrometry proteome and acetylome data have been deposited to the ProteomeXchange Consortium (<https://proteomecentral.proteomexchange.org>) via the iProX partner repository [46, 47] with the dataset identifier PXD056800.

URL:<https://www.iprox.cn/page/PSV023.html?url=1728976654485D9GS>.  
Password: q3wg.

## Declarations

### Ethics approval and consent to participate

This work have been performed according to the Declaration of Helsinki, informed consent was obtained for all subjects. The procedures have been approved by the ethical committee of Plastic Surgery Hospital, Chinese Academy of Medical Sciences and Peking Union Medical College (Project number: 2024ZXLHWT07; Serial number of auditing: 2024 Registration NO. (192)).

### Consent for publication

Not applicable.

### Competing interests

The authors declare no competing interests.

### Author details

<sup>1</sup>The Centre for Cleft Lip and Palate Treatment, Plastic Surgery Hospital, Chinese Academy of Medical Sciences and Peking Union Medical College, 33 Badachu Road, Shijingshan District, Beijing 100144, People's Republic of China

<sup>2</sup>State Key Laboratory of Medical Molecular Biology, Department of Biochemistry and Molecular Biology, Institute of Basic Medical Sciences, Chinese Academy of Medical Sciences & Peking Union Medical College, Beijing, China

<sup>3</sup>The Center for Obesity and Metabolic Disease, Plastic Surgery Hospital, Chinese Academy of Medical Sciences and Peking Union Medical College, 33 Badachu Road, Shijingshan District, Beijing 100144, People's Republic of China

Received: 14 November 2024 / Accepted: 18 January 2025

Published online: 29 January 2025

## References

- World Obesity Federation. World obesity Atlas 2024. London: World Obesity Federation; 2024.
- Alberti KG, Zimmet P, Shaw J, IDF Epidemiology Task Force Consensus Group. The metabolic syndrome—a new worldwide definition. *Lancet*. 2005 Sep;24–30(9491):1059–62.

3. Katzmarzyk PT, Church TS, Janssen I, Ross R, Blair SN. Metabolic syndrome, obesity, and mortality: impact of cardiorespiratory fitness. *Diabetes Care*. 2005;28(2):391–7.
4. Dagpo TD, Nolan CJ, Delghingaro-Augusto V. Exploring therapeutic targets to reverse or prevent the transition from metabolically healthy to unhealthy obesity. *J Cell Physiol*. 2020;9(7):1596.
5. Zwick RK, Guerrero-Juarez CF, Horsley V, Plikus MV. Anatomical, physiological, and functional diversity of adipose tissue. *Cell Metab*. 2018;27(1):68–83.
6. Ibrahim MM. Subcutaneous and visceral adipose tissue: structural and functional differences. *Obes Rev*. 2010;11(1):11–8.
7. Ravussin E, Smith SR. Increased fat intake, impaired fat oxidation, and failure of fat cell proliferation result in ectopic fat storage, insulin resistance, and type 2 diabetes mellitus. *Ann NY Acad Sci*. 2002;967:363–78.
8. Jensen MD. Adipose tissue and fatty acid metabolism in humans. *J R Soc Med*. 2002;95(42):3–7.
9. Cypess AM. Reassessing human adipose tissue. *N Engl J Med*. 2022;386(8):768–79.
10. Kim EY, Kim WK, Oh KJ, Han BS, Lee SC, Bae KH. Recent advances in proteomic studies of adipose tissues and adipocytes. *Int J Mol Sci*. 2015;16(3):4581–99.
11. Pérez-Pérez R, Ortega-Delgado FJ, García-Santos E, et al. Differential proteomics of omental and subcutaneous adipose tissue reflects their unlike biochemical and metabolic properties. *J Proteome Res*. 2009;8(4):1682–93.
12. Hruska P, Kucera J, Pekar M, et al. Proteomic Signatures of Human Visceral and subcutaneous adipocytes. *J Clin Endocrinol Metab*. 2022;107(3):755–75.
13. Murri M, Insenser M, Bernal-Lopez MR, Perez-Martinez P, Escobar-Morreale HF, Tinahones FJ. Proteomic analysis of visceral adipose tissue in pre-obese patients with type 2 diabetes. *Mol Cell Endocrinol*. 2013;376(1–2):99–106.
14. Carruthers NJ, Strieder-Barboza C, Caruso JA, et al. The human type 2 diabetes-specific visceral adipose tissue proteome and transcriptome in obesity. *Sci Rep*. 2021;11(1):17394.
15. Xie X, Yi Z, Bowen B, Wolf C, Flynn CR, Sinha S, Mandarin LJ, Meyer C. Characterization of the human adipocyte proteome and reproducibility of protein abundance by one-dimensional gel electrophoresis and HPLC-ESI-MS/MS. *J Proteome Res*. 2010;9(9):4521–34.
16. Kim SJ, Chae S, Kim H, Mun DG, et al. A protein profile of visceral adipose tissues linked to early pathogenesis of type 2 diabetes mellitus. *Mol Cell Proteom*. 2014;13(3):811–22.
17. Pérez-Pérez R, García-Santos E, Ortega-Delgado FJ, et al. Attenuated metabolism is a hallmark of obesity as revealed by comparative proteomic analysis of human omental adipose tissue. *J Proteom*. 2012;75(3):783–95.
18. Mardinoglu A, Kampf C, Asplund A, et al. Defining the human adipose tissue proteome to reveal metabolic alterations in obesity. *J Proteome Res*. 2014;13(11):5106–19.
19. Liu Y, Yang H, Liu X, Gu H, Li Y, Sun C. Protein acetylation: a novel modus of obesity regulation. *J Mol Med (Berl)*. 2021;99(9):1221–35.
20. Yang H, Yang K, Gu H, Sun C. Dynamic post-translational modifications in obesity. *J Cell Mol Med*. 2020;24(3):2384–7.
21. Navarro-Ruiz MDC, López-Alcalá J, Díaz-Ruiz A, et al. Understanding the adipose tissue acetylome in obesity and insulin resistance. *Transl Res*. 2022;246:15–32.
22. Executive Summary of The Third Report of The National Cholesterol Education Program (NCEP). Expert Panel on detection, evaluation, and treatment of high blood cholesterol in adults (Adult Treatment Panel III). *J Am Med Assoc*. 2001;285:2486–97.
23. Hruska P, Kucera J, Kuruczova D, et al. Unraveling adipose tissue proteomic landscapes in severe obesity: insights into metabolic complications and potential biomarkers. *Am J Physiol Endocrinol Metab*. 2023;325(5):E562–80.
24. Després JP, Lemieux I. Abdominal obesity and metabolic syndrome. *Nature*. 2006;444(7121):881–7.
25. Longo M, Zatterale F, Naderi J, et al. Adipose tissue dysfunction as determinant of obesity-Associated Metabolic complications. *Int J Mol Sci*. 2019;20(9):2358.
26. Tchakonia T, Thomou T, Zhu Y, et al. Mechanisms and metabolic implications of regional differences among fat depots. *Cell Metab*. 2013;17:644–56.
27. Mariman EC, Wang P. Adipocyte extracellular matrix composition, dynamics and role in obesity. *Cell Mol Life Sci*. 2010;67(8):1277–92.
28. Nakajima I, Muroya S, Tanabe R, Chikuni K. Extracellular matrix development during differentiation into adipocytes with a unique increase in type V and VI collagen. *Biol Cell*. 2002;94(3):197–203.
29. Mishra YG, Manavathi B. Focal adhesion dynamics in cellular function and disease. *Cell Signal*. 2021;85:110046.
30. Khan T, Muise ES, Iyengar P, et al. Metabolic dysregulation and adipose tissue fibrosis: role of collagen VI. *Mol Cell Biol*. 2009;29(6):1575–91.
31. Fruman DA, Chiu H, Hopkins BD, Bagrodia S, Cantley LC, Abraham RT. The PI3K pathway in Human Disease. *Cell*. 2017;170(4):605–35.
32. Savova MS, Mihaylova LV, Tews D, Wabitsch M, Georgiev MI. Targeting PI3K/AKT signaling pathway in obesity. *Biomed Pharmacother*. 2023;159:114244.
33. Kobayashi N, Ueki K, Okazaki Y, et al. Blockade of class IB phosphoinositide-3 kinase ameliorates obesity-induced inflammation and insulin resistance. *Proc Natl Acad Sci U S A*. 2011;108(14):5753–8.
34. Krupka S, Hoffmann A, Jasaszwilli M, Dietrich A, Guiu-Jurado E, Klötting N, Blüher M. Consequences of COVID-19 on adipose tissue signatures. *Int J Mol Sci*. 2024;25(5):2908.
35. Pasarica M, Gowronska-Kozak B, Burk D, et al. Adipose tissue collagen VI in obesity. *J Clin Endocrinol Metab*. 2009;94:5155–62.
36. Morandi EM, Verstappen R, Zwierzina ME, Geley S, Pierer G, Ploner C. ITGA5 and ITGA5 diversely regulate proliferation and adipogenic differentiation of human adipose derived stem cells. *Sci Rep*. 2016;6:28889.
37. Cui K, Ardell CL, Podolnikova NP, Yakubenko VP. Distinct migratory properties of M1, M2, and resident macrophages are regulated by aDb2 and aMb2 integrin-mediated adhesion. *Front Immunol*. 2018;9:2650.
38. Larsen JK, Kruse R, Sahebkhari N, et al. High-throughput proteomics uncovers exercise training and type 2 diabetes-induced changes in human white adipose tissue. *Sci Adv*. 2023;9(48):eadi7548.
39. Zhou Y, Peng J, Jiang S. Role of histone acetyltransferases and histone deacetylases in adipocyte differentiation and adipogenesis. *Eur J Cell Biol*. 2014;93(4):170–7.
40. Małodobra-Mazur M, Cierznia A, Myszczyzyn A, Kaliszewski K, Dobosz T. Histone modifications influence the insulin-signaling genes and are related to insulin resistance in human adipocytes. *Int J Biochem Cell Biol*. 2021;137:106031.
41. Andrés M, García-Gomis D, Ponte I, Suau P, Roque A. Histone H1 post-translational modifications: update and future perspectives. *Int J Mol Sci*. 2020;21(16):5941.
42. van den Jacob D, Sandbäck P, Brenda JM, Pisa I, Eriksson L, Kjellén, Jo HM, Berden. January, Antibody-based assay for N-deacetylase activity of heparan sulfate/heparin N-deacetylase/N-sulfotransferase (NDST): novel characteristics of NDST-1 and -2. *Glycobiology*, 13, Issue 1, 2003, Pages 1–10.
43. Otsuka T, Kan HM, Mason TD, Nair LS, Laurencin CT. Overexpression of NDST1 attenuates fibrotic response in murine adipose-derived stem cells. *Stem Cells Dev*. 2022;31(23–24):787–98.
44. Reinisch I, Ghosh A, Noé F et al. Unveiling adipose populations linked to metabolic health in obesity. *Cell Metab* 2024 Dec 11;S1550-4131(24)00452–2.
45. Alfadda AA, Masood A, Al-Naami MY, Chaurand P, Benabdelkamel H. A Proteomics Based Approach reveals Differential Regulation of visceral adipose tissue proteins between metabolically healthy and unhealthy obese patients. *Mol Cells*. 2017;40(9):685–95.
46. Ma J, et al. iProX: an integrated proteome resource. *Nucleic Acids Res*. 2019;47(D1):D1211–7.
47. Chen T, et al. iProX in 2021: connecting proteomics data sharing with big data. *Nucleic Acids Res*. 2021;50(D1):D1522–7.

## Publisher's note

Springer Nature remains neutral with regard to jurisdictional claims in published maps and institutional affiliations.